Materials Research Express

PAPER

Control of PbI_2 nucleation and crystallization: towards efficient perovskite solar cells based on vapor-assisted solution process

Materials Research Express

PAPER

Control of PbI_2 nucleation and crystallization: towards efficient perovskite solar cells based on vapor-assisted solution process

Chongqiu Yang[1,2,4], **Yanke Peng**[2,3], **Terrence Simon**[2] and **Tianhong Cui**[2,4]

[1] School of Mechatronics Engineering, Harbin Institute of Technology, Harbin 150001, People's Republic of China
[2] Department of Mechanical Engineering, University of Minnesota, Minneapolis, MN 55455, United States of America
[3] State Key Laboratory of Precision Measurement Technology and Instruments, Department of Precision Instruments, Tsinghua University, Beijing, 100084, People's Republic of China
[4] Authors to whom any correspondence should be addressed.

E-mail: yangchongqiu@hotmail.com **and** tcui@me.umn.edu

Keywords: perovskite, solar cell, lead iodide

RECEIVED
21 February 2018

REVISED
21 March 2018

ACCEPTED FOR PUBLICATION
22 March 2018

PUBLISHED
13 April 2018

Abstract

Perovskite solar cells (PSC) have outstanding potential to be low-cost, high-efficiency photovoltaic devices. The PSC can be fabricated by numerous techniques; however, the power conversion efficiency (PCE) for the two-step-processed PSC falls behind that of the one-step method. In this work, we investigate the effects of relative humidity (RH) and dry air flow on the lead iodide (PbI_2) solution deposition process. We conclude that the quality of the PbI_2 film is critical to the development of the perovskite film and the performance of the PSC device. Low RH and dry air flow used during the PbI_2 spin coating procedure can increase supersaturation concentration to form denser PbI_2 nuclei and a more suitable PbI_2 film. Moreover, airflow-assisted PbI_2 drying and thermal annealing steps can smooth transformation from the nucleation stage to the crystallization stage.

1. Introduction

Development of perovskite solar cells has shown impressive progress in just a few years, recently yielding a certified maximum power conversion efficiency of 22.1% [1]. This rapid and dramatic improvement sets it apart from conventional solar cells, such as silicon and copper indium gallium selenide cells [2]. Perovskite films can be obtained by many techniques, including solution process (one-step spin coating [3, 4], two-step spin coating [5] or dipping [6]), vapor-assisted solution process [7–9], and dual vapor deposition[10–13]. However, the vapor-assisted solution process is more easily controlled in balancing film growth, morphology, grain structure of PbI_2 and perovskite film thickness [14–16]. PbI_2 and perovskite layer growth are separated into two independent stages, although their film qualities are strongly correlated. Vapor-assisted crystal growth enables homogeneous perovskite films with fewer defects and well-defined grain structures, suitable for photovoltaic applications [15].

To obtain excellent performance of a PSC, uniform and dense perovskite films with excellent crystal quality must be grown. For the vapor-assisted solution process, perovskite $CH_3NH_3PbI_3$ ($MAPbI_3$) formation can be regarded as an intercalation reaction between a precursor PbI_2 crystal film and vapor of CH_3NH_3I (MAI) [17]. Therefore, the perovskite film is primarily determined by the PbI_2 precursor film and the chemical vapor deposition (CVD) process. Our previous work indicated that the homogeneous perovskite crystallization process can be precisely managed by control of the temperature, pressure, time, vapor transport and diffusion during CVD deposition [18]. Much work has shown that the morphology and precursor solution of PbI_2 significantly influence the perovskite. Cao *et al* [17, 19] and Yin *et al* [7] introduced a strong Lewis-base additive to the PbI_2/DMF precursor solution to get a porous PbI_2 morphology, to facilitate fully the intercalation reaction. Wu *et al* [20] obtained a high quality PbI_2 film with full coverage by adding a controllable amount of water in the PbI_2/DMF solution. The final perovskite film was highly pure, smooth and dense, and without a single pinhole. Liu *et al* [21] developed a mesoporous PbI_2 scaffold by delicate nucleation control, showing

controllable influences on crystallization of the perovskite film. Hwang *et al* [22] adopted a slot-die coating with a gas quenching process for fabrication of a pinhole-free PbI_2 layer, and indicated that the perovskite solar cell performance was strongly dependent on the PbI_2 layer morphology.

Relative humidity (RH) is reported as a significant factor influencing perovskite film formation and degradation when using the one-step spin coating process [23]. Gao *et al* [24] investigated the influence of ambient humidity (RH 1% $\sim$ RH 70%) on crystallization and surface morphology of the one-step, spin-coating process for perovskite $MAPbI_3$ films and found that the uniformity of coverage of the perovskite film decreases obviously with increasing RH. Wozny *et al* [25] observed similar phenomena in the one-step, spin-coated formamidinium (FA)-based perovskite film. Additionally, dry gas flow (air, argon, or nitrogen) was introduced in the one-step deposition method to get full-coverage and smooth perovskite films [26–28]. For the two-step deposition method, since the completed perovskite film structure and the eventual solar cell performance are strongly dependent on the precursor PbI_2 film, the effects of RH and gas flow during the PbI_2 film growth must be addressed.

Here, we aim to clarify the role of RH and air flow on PbI_2 nucleation and crystallization during the spin coating, drying, and annealing stages. It is found that spin coating PbI_2 films at different RH levels can influence the morphology of the perovskite film, resulting in different PCE values. A lower RH facilitates solvent evaporation during spinning to achieve a higher PbI_2 supersaturation concentration. This increased supersaturation promotes growth of uniform PbI_2 nuclei and full-coverage growth of the layer [29], enabling homogeneous perovskite layer growth. Further study indicates that airflow-assisted spinning followed by drying steps can increase supersaturation concentration to get more uniform PbI_2 nuclei coverage. Moreover, since thermal annealing is always done with the hot plate set at $\sim$100 °C, while the airflow is introduced at room temperature, airflow assisted annealing can slow the PbI_2 crystallization rate to relieve the crystal stress. A uniform and defect-free PbI_2 film benefits the perovskite film growth and PSC performance.

2. Experimental methods

2.1. Device fabrication

The laser-patterned FTO glass (Tec15, Pilkington) was sequentially ultrasonically cleaned with deionized water, acetone, and isopropyl alcohol (IPA), followed by ultraviolet ozone treatment. Next, a compact TiO_2 layer was deposited by spin coating 0.15 M titanium diisopropoxide bis (acetylacetonate) (75 wt.% in isopropanol, Sigma-Aldrich) in anhydrous ethanol ($\geqslant$99.5%, Sigma-Aldrich) twice at 4000 rpm for 30 s, drying at 125 °C for 5 min, and annealing at 500 °C in air for 45 min. Perovskite films were grown by the two-step, vapor-assisted solution process. A 1M PbI_2 (>99.99%, Xi'an Polymer Light Technology, China) solution in *N*,*N*-Dimethylformamide (DMF, anhydrous, 99.8%, Sigma-Aldrich) and Dimethyl sulfoxide (DMSO, anhydrous, $\geqslant$99.9%, Sigma-Aldrich) (DMF:DMSO = 4:1) was spin-coated on the TiO_2 at 4000 rpm for 30 s, and then annealed at 100 °C for 10 min. For the airflow-assisted PbI_2 deposition process, an air flow with supply pressure of 69 kPa (10 psi) was introduced during the spinning (10 s after spinning started), the drying, or the annealing stages. The PbI_2 substrates were transferred to the vapor deposition chamber designed and built in the UMN lab (inner diameter of 40 mm, length of 200 mm, figure 1). MAI powder ($\geqslant$99.5%, Xi'an Polymer Light Technology, China) in transparent quartz crucibles was placed in the chamber regularly to obtain a uniform vapor flow distribution to grow a homogeneous perovskite film [18]. The chamber was transferred to the middle-zone of a commercial, single-zone CVD furnace chamber (inner diameter of 120 mm, heating zone length of 880 mm, MTI Corporation). The vapor deposition process of the perovskite film was conducted at 110 °C for 7 h with a vacuum of $\sim$3 mTorr. The hole-transporting layer was deposited on the perovskite film by spin coating a solution of spiro-MeOTAD (72.3 mg, Lumtech, Taiwan) mixed with 4-*tert*-butyl pyridine (28.8 μl, Sigma-Aldrich) and lithium bis (trifluoromethanesulfonyl) imide solution (17.5 μl, Li-TFSI, 520 mg Li-TSFI in 1 ml acetonitrile, Sigma-Aldrich) in chlorobenzene (1 ml, Sigma-Aldrich) at 4000 rpm for 30 s. Finally, silver electrodes of 70 nm were deposited by thermal evaporation through a shadow mask. The active area of the complete device was 0.09 cm^2. All devices were fabricated in ambient air.

2.2. Characterization

The surface and cross-section morphologies were investigated by a Field Emission Gun Scanning Electron Microscope (SEM, JEOL 6500). The crystallinity of the perovskite films was characterized by x-ray diffraction (XRD, Bruker-AXS D5005, Siemens). Current density–voltage (J–V) measurements of the solar cells were performed by an electrochemical detection workstation (CHI 630C). The AM 1.5 G illumination (100 mW cm^{-2}) was generated by a xenon-based, Newport Co. simulator (67005), calibrated by a Newport Co. radiant power meter (70260) and probe (70268).

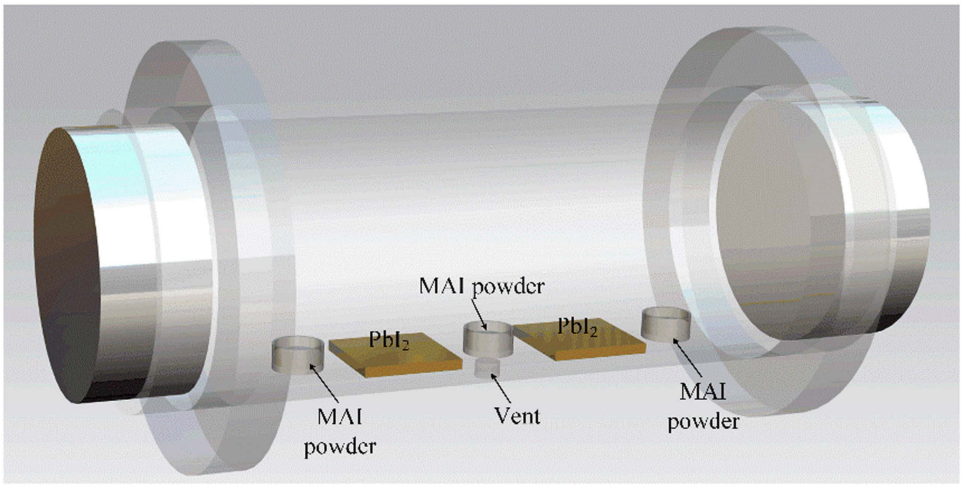

Figure 1. PbI_2 substrates and MAI powder in lab-fabricated, vapor deposition chamber.

3. Results and discussion

3.1. Spin-coating PbI_2 at various relative humidity (RH) values

Developing a uniform and dense perovskite film is critical to achieving good performance in perovskite solar cells. Relative humidity is reported to be a factor influencing perovskite film growth and affecting PCE performance and stability of perovskite solar cells [30, 31]. Here, we propose that RH also influences PbI_2 film growth and determines the resultant perovskite film quality and final device performance.

Figure 2 presents surface morphologies of PbI_2 and perovskite films. A layer of PbI_2 was spin-coated at various RH levels then allowed to react to form perovskite using a modified CVD process, as discussed in the Experimental section. Using DMSO and DMF as solvents to the PbI_2, the surface is formed with the morphology shown in figures 2(a) and (b). This is consistent with reports in the literature [6, 17, 32]. Porous PbI_2 is beneficial for it allows vapor MAI to penetrate its deep sites to ensure a complete transformation reaction of the perovskite. At a high RH of 55%, PbI_2, the surface shows large porous holes with indistinguishable block grain crystals, figure 2(a). As the RH is decreased to 16%, figure 2(b), smaller voids become visible on the PbI_2 surface and small-grain crystals can be recognized. The resulting CVD-processed perovskite films also show differences. Figure 2(c) presents the perovskite film grown from a 55% RH-deposited PbI_2 layer. Discontinuous cracks between small perovskite grain boundaries appear. As shown in figures 2(d)–(f), PbI_2 layers deposited with RH $\leqslant$ 45% develop uniform and continuous, small perovskite grains.

Figure 3 shows the *J–V* curves of PSCs prepared from PbI_2 layers deposited under different RH values. Corresponding photovoltaic performance values are presented in table 1. As the RH decreases, the PCE of the PSC devices increases rapidly. With a RH of 55%, the filling factor of the *J–V* curves is low due to poor perovskite film quality, as shown in figure 2(c). Moreover, the discontinuous cracks prompt recombination of holes and electrons, reducing low open-circuit voltage. When the RH is lower than 45%, V_{oc} stabilizes at ~0.9 V, consistent with the uniform and dense perovskite surface morphologies in figure 2. While at the lower RH, better grain crystals of PbI_2 and improved perovskite films enhance light absorption to increase current density. Hysteresis of *J–V* is a notorious phenomenon in planar PSCs. It is caused by surface and bulk defects and ion migration in the perovskite film, as reported [33, 34]. The defects could act as traps for electrons or holes, filling and emptying with forward and reverse scans [35]. PCBM is reported to passivate and reduce the defects efficiently, leading to negligible hysteresis [36, 37]. However, the exact physical mechanisms associated with PCBM were not fully studied. For example, the potential PCBM-related reduction of ion migration at grain boundaries could also be a reason for minimizing *J–V* hysteresis [34]. Some theoretical and experimental studies showed that I^- ions are easily photo-activated or electro-activated to move through grain boundaries. The accumulation of ions at the interfaces might further enhance the generation of local defects in the lattice, resulting in an enhancement of ion movement through drift and diffusion [33, 38, 39]. More study is needed to identify and resolve this notorious issue, and no further discussion is given in this paper. A serious hysteresis exists in some devices of the present study, even for the 16% RH-deposited PbI_2 device, as shown in figure 3(b).

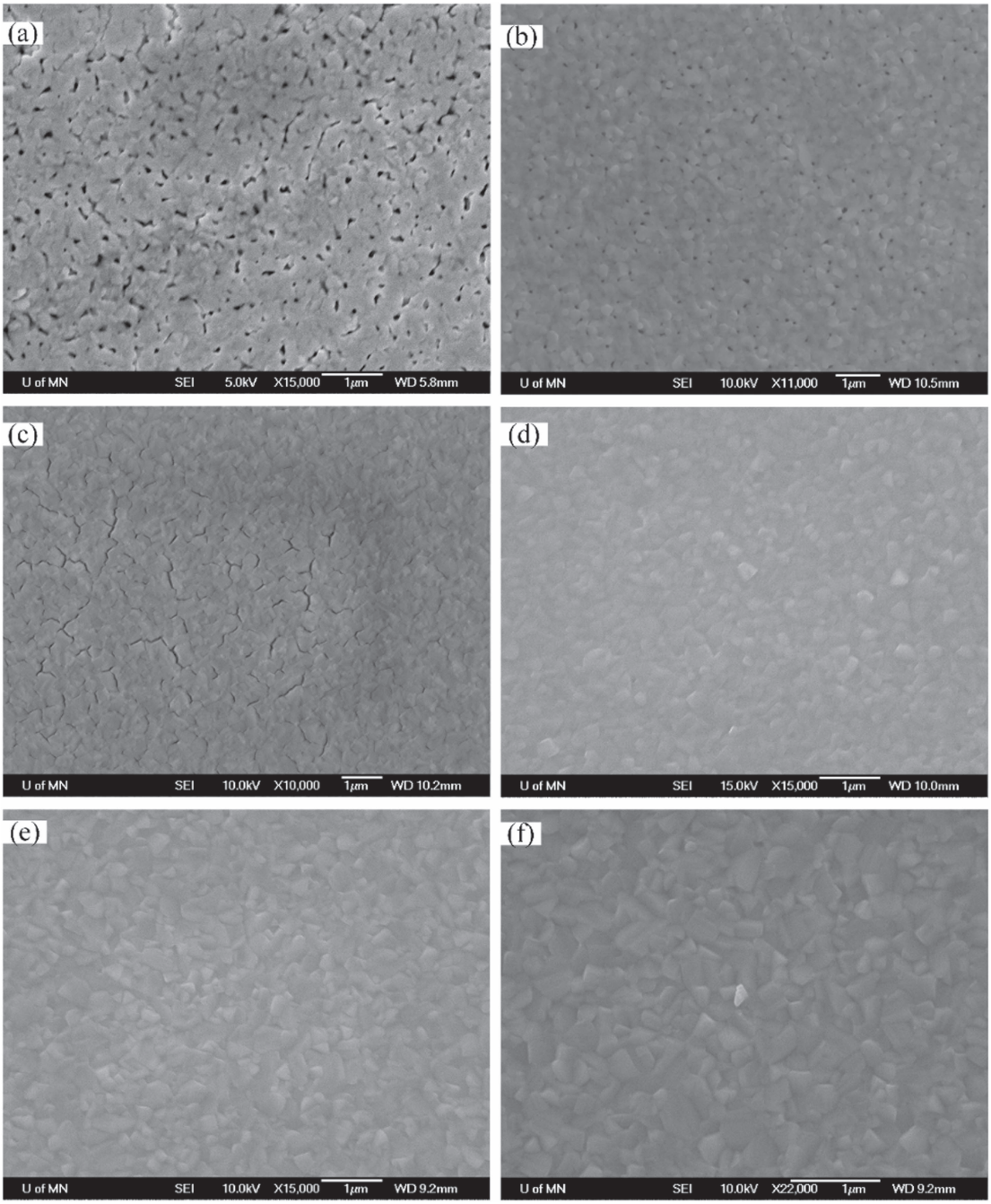

Figure 2. SEM surface morphologies of PbI_2 films spin-coated at different RHs: (a) 55% RH, (b) 16% RH. SEM surface morphologies of perovskite films grown from spin-coated PbI_2 at various RHs: (c) 55% RH, (d) 45% RH, (e) 35% RH, (f) 16% RH.

3.2. Airflow-assisted PbI_2 deposition processes

Figure 4 illustrates the airflow-assisted PbI_2 deposition process, including corresponding photographs for each step. Solvents of PbI_2 solution are DMF and DMSO. Wu *et al* [6] showed that a DMSO-based, fresh-spun PbI_2 film with light yellow color maintains its non-crystallized amorphous feature, certified by the absorption and XRD characterization. Here, as shown in figure 4, the spin-coated and further dried PbI_2 films with airflow assistance maintains a light yellow color, indicating its amorphous feature. In the next step, the PbI_2 film still keeps its light yellow color even with airflow-assisted thermal annealing at 100 °C. The deposited PbI_2 layer can be quickly transferred to a deep yellow color in 1 min using a conventional thermal annealing step without airflow assistance, as shown in the fourth photograph in figure 4. Essentially, airflow assistance delays the color change or delays the conversion of PbI_2 from an amorphous state to a crystallized state during thermal annealing. It is proposed that room-temperature airflow retards the heating effect on a PbI_2 film, slowing down its crystallization rate.

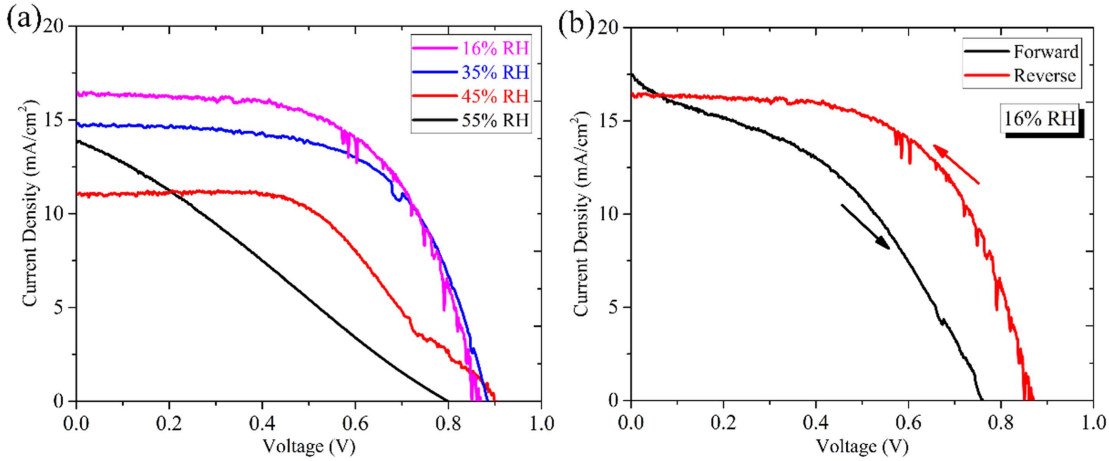

Figure 3. (a) Reverse-scanned *J–V* curves of PSCs prepared from different PbI_2 films deposited under different RH values (b) *J–V* curve hysteresis of PSC prepared by spinning PbI_2 at 16% RH.

Table 1. Photovoltaic performance of PSC devices shown in figure 3.

	J_{sc} (mA cm^{-2})	V_{oc} (V)	FF	PCE
55% RH	13.88	0.8	0.27	3%
45% RH	11.06	0.9	0.52	5.2%
35% RH	14.78	0.88	0.61	8%
16% RH Reverse	16.5	0.87	0.60	8.55%
16% RH Forward	17.5	0.76	0.41	5.48%

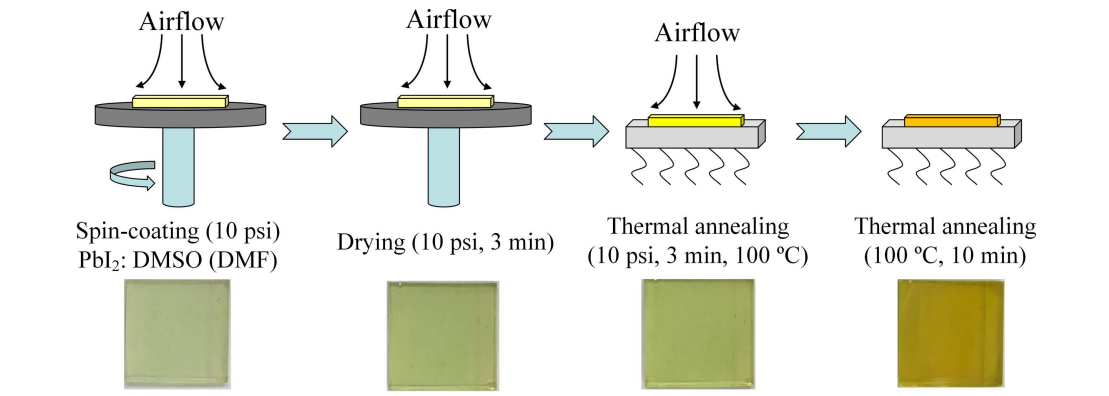

Figure 4. Schematic illustration and corresponding photographs of the airflow-assisted PbI_2 deposition process.

The airflow-assisted, spin-deposited PbI_2 film was converted to a perovskite film by the CVD process, as discussed in the Experimental section. The crystallinity of each perovskite film was characterized by an XRD curve, as shown in figure 5(a). The absence of PbI_2 diffraction peaks in all the XRD curves indicates that the PbI_2 was fully reacted to produce perovskite crystals. The perovskite diffraction peaks are consistent with reports in the literature [6, 32]. Using a conventional PbI_2 deposition process, without airflow assistance, we see that the (110) peak of the as-grown perovskite film is the lowest of the group (black curve in figure 5(a)), indicating its poor crystallinity. In accordance with its surface morphology, as shown in figure 5(b), the perovskite film shows incomplete coverage with large pinholes and indistinguishable grain crystals. The airflow then was introduced during the PbI_2 spin coating procedure and the XRD peak of the as-grown perovskite film increased greatly (red curve in figure 5(a)). Also, the perovskite film showed dense crystal grains with small pinholes, see figure 5(c). Using a conventional spin-coated PbI_2 film, but adding an airflow-assisted drying step yielded an XRD peak for the CVD-processed perovskite film that is improved significantly (blue curve in figure 5(a)). The surface-SEM image in figure 5(d) shows a well-covered perovskite film without pinholes, but also shown are small cracks between grain boundaries. Coupling with an airflow-assisted thermal annealing step following the conventional

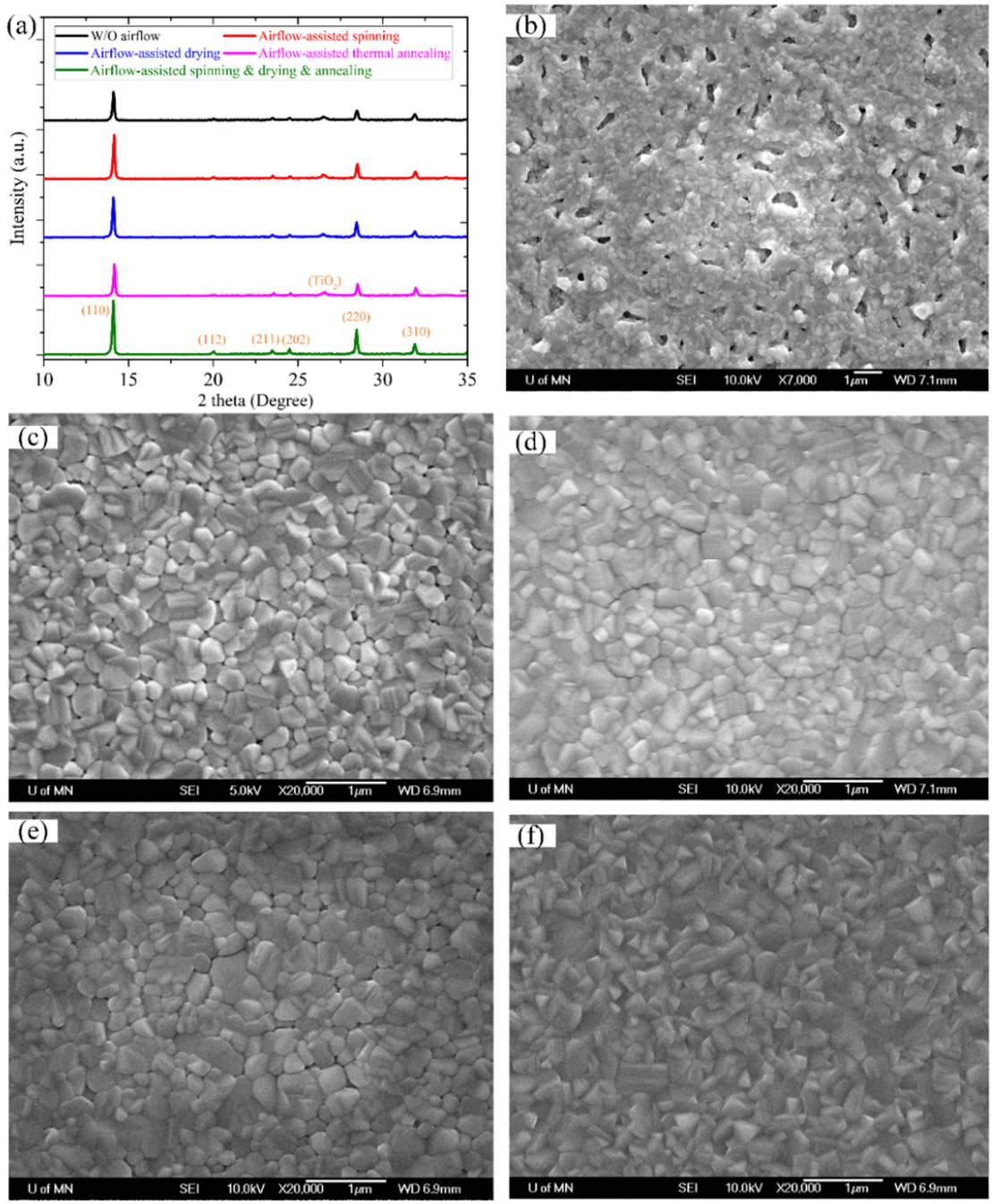

Figure 5. (a) XRD curves of PSC prepared from various PbI_2 films by airflow-assisted spinning, drying and thermal annealing at 55% RH. The corresponding SEM surface morphologies: (b) Without airflow-assist, (c) With airflow-assisted spinning, (d) With airflow-assisted drying, (e) With airflow-assisted thermal annealing, (f) With airflow-assisted spinning, drying, and thermal annealing.

PbI_2 spin coating process, the XRD peak intensity of as-grown perovskite film did not change significantly (pink curve in figure 5(a)). However, the SEM picture of the as-grown perovskite film in figure 5(e) shows greatly improved surface coverage compared with figure 5(b), although the grain crystals are not dense enough, with large grain boundaries and small pinholes. If airflow is introduced during the PbI_2 spinning, drying and thermal annealing stages, a perovskite film with the largest XRD peak intensity of the group is obtained and crystallinity is optimum (lowest green curve in figure 5(a)). The surface morphology also shows dense and uniform perovskite grain crystals without pinholes, as shown in figure 5(f). As for the crystallinity of the resultant PbI_2 film, airflow assistance or low relative humidity can generate more PbI_2 nuclei, and the grown PbI_2 crystals are small and dense (figure 2(b)), and the corresponding PbI_2 crystallinity would be limited. However, the crystallinity and surface morphology of the reacted perovskite films are increased according to the figures 5(a) and (f), mainly due to the homogeneous reaction with growth from uniformly-distributed PbI_2 nuclei.

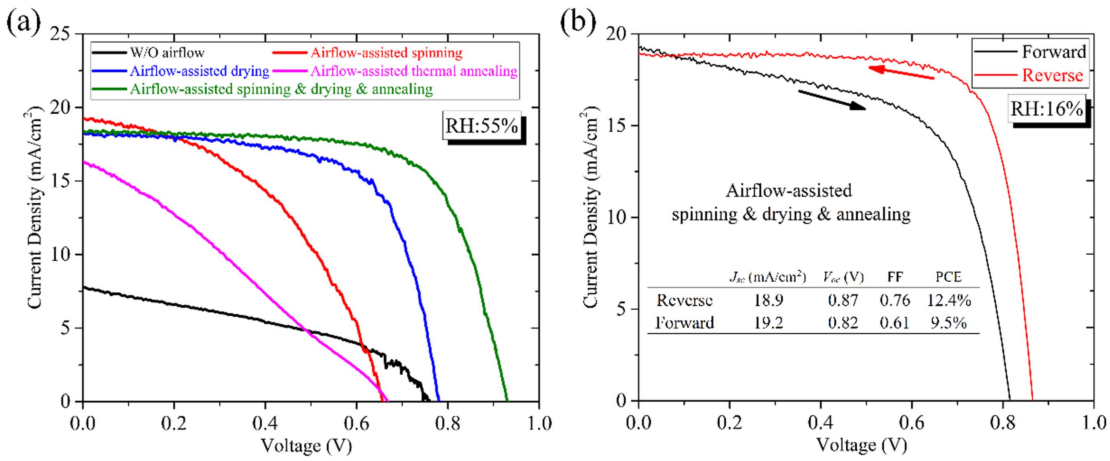

Figure 6. (a) Reverse-scanned *J–V* curves of PSC prepared from various PbI_2 films by airflow-assisted spinning, drying, or thermal annealing at 55% RH. (b) *J–V* curve for the device prepared by airflow-assisted PbI_2 spinning, drying, and thermal annealing at 16% RH.

Table 2. Photovoltaic performance of the PSC devices shown in figure 6(a).

	J_{sc} (mA cm^{-2})	V_{oc} (V)	FF	PCE
Without airflow	7.78	0.76	0.4	2.4%
Airflow-assisted spinning	19.2	0.66	0.46	5.8%
Airflow-assisted drying	18.24	0.78	0.67	9.5%
Airflow-assisted thermal annealing	16.3	0.67	0.28	3.1%
Airflow-assisted spinning, drying and thermal annealing	18.42	0.93	0.69	11.8%

The photovoltaic performance of PSC prepared from various airflow-assisted PbI_2 films is presented in figure 6 and table 2. The PSC based on the conventional PbI_2 deposition process without airflow assist shows very low J_{sc} and PCE, due to incomplete coverage of the perovskite film, cutting down light absorption in the layer. In addition, the poor perovskite crystallinity and large pinholes increase the inner resistance and enhance recombination of holes and electrons, deteriorating the FF and V_{oc}. The J_{sc} increases greatly after introducing airflow to the PbI_2 deposition process, consistent with the full-coverage perovskite film (figure 5), leading to increased efficiency of absorbing light. Simply introducing airflow during PbI_2 spinning or thermal annealing steps is not sufficient, the V_{oc} and FF are not sufficient due to perovskite crystals with pinholes (figures 5(c) and (e)).

The airflow-assisted PbI_2 drying procedure seems to be essential to getting a perovskite film or PSC with good photovoltaic performance, especially as seen in the FF values, consistent with the large XRD peak intensity and dense perovskite surface quality. Further improved performance of PSC is obtained by adding airflow into the spinning, drying, and thermal annealing steps, as illustrated in figure 4. When the PbI_2 deposition process was operated at high RH of 55%, a PCE of 11.8% was attained (J_{sc} 18.42 mA cm^{-2}, V_{oc} 0.93 V and FF 0.69). While at low RH of 16%, a PCE of 12.4% was achieved with a high FF of 0.76, though with a large hysteresis.

Figure 7 illustrates the concentration changes during the airflow-assisted PbI_2 deposition process. Generally, thin film growth involves two stages: nucleation and crystallization. Supersaturation is the driving potential for precipitating PbI_2 atoms, and, with higher supersaturation, a larger number of nuclei form on the substrate to capture more atoms for growing crystals. Figure 7 shows that in a conventional PbI_2 deposition process, without airflow assistance (a), high-speed spin coating causes the PbI_2 precursor solution to enter a limited supersaturation state. Then, high temperature annealing actives a fast-crystallization process. According to thin film growth theory, increased supersaturation is necessary to form uniformly-distributed nuclei and smooth layer growth [29, 40]. The solvents of PbI_2, DMF and DMSO, prefer to absorb water. Therefore, spin coating at high RH may increase the partial pressure of solvent DMF and DMSO in the ambient air, deteriorating solvent evaporation. The supersaturation concentration of the PbI_2 solution is then retarded, causing fewer nucleation sites and aggregated crystal growth with large pinholes, as shown in figure 2(a). This poor PbI_2 film generates an incompletely-covered perovskite film, as shown in figures 2(c) and 5(b). Airflow assisting during the spin coating step can hasten solvent evaporation rate, even at a RH of 55%, achieving a higher concentration of supersaturation and allowing the formation of more PbI_2 nuclei on the substrate. The resulting CVD-processed

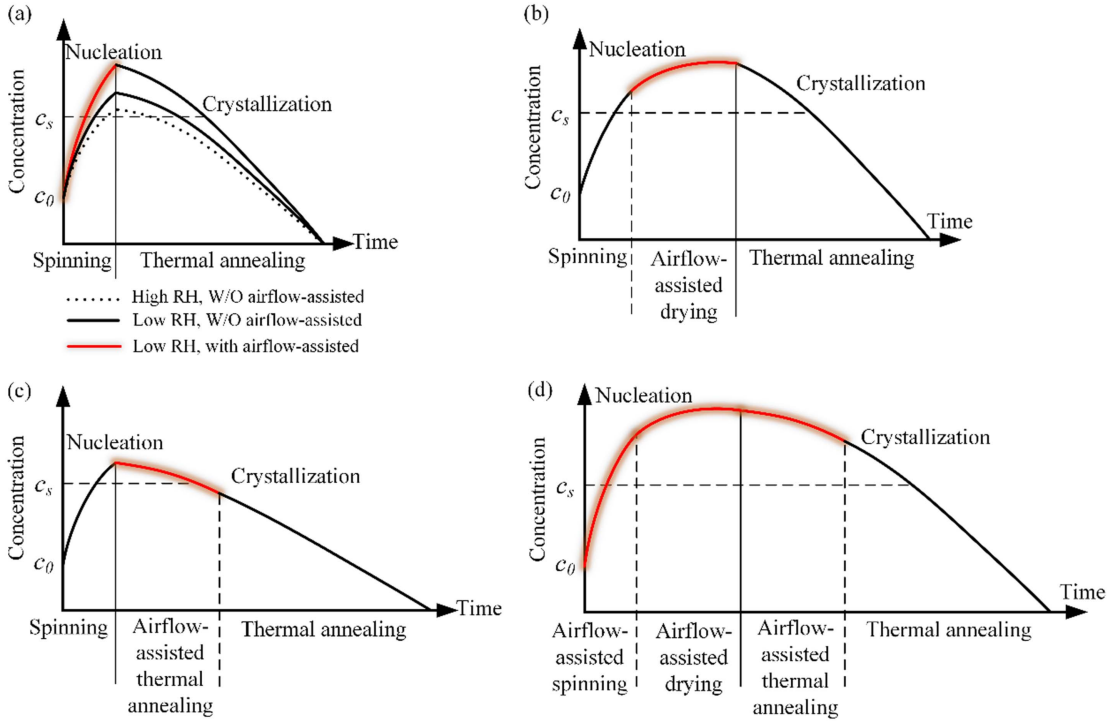

Figure 7. Schematic illustration of solution concentration during the nucleation and crystallization processes of a PbI_2 film. The red shadowed curves represent the airflow-assisted procedure and the black curves represent a conventional procedure without airflow assisting. The continuous lines represent low RH-processed PbI_2, and the dash lines represent high RH-processed PbI_2. The concentration of precursor solution is c_0 and c_s is the concentration of saturation. (a) Without or with airflow-assisted spinning, (b) With airflow-assisted drying, (c) With airflow-assisted thermal annealing, (d) With airflow-assisted spinning, drying and thermal annealing.

perovskite film shows better coverage, see figure 5(c). Airflow-assisted drying of a spin-coated PbI_2 film can further increase supersaturation by evaporating more solvent, as shown in figure 7(b). Increased supersaturation can generate more uniform PbI_2 nuclei and benefit the subsequent growth of dense perovskite crystals, as shown in figure 5(d). Moreover, according to the concentration curve in figure 7(b), airflow-assisted drying can smooth the curvature variation and the corresponding PbI_2 transformation from the nucleation stage to the crystallization stage due to increased supersaturation. Figure 7(c) presents the effect of airflow-assisted thermal annealing on the concentration variation of a PbI_2 solution. As discussed before, room temperature airflow can retard the heating effect on as-deposited PbI_2 films, slowing down the crystal growth rate. For the optimized procedure, with airflow assisting in all spinning, drying, and thermal annealing steps, a very smooth concentration variation curve is found (figure 7(d)). High supersaturation concentration at the nucleation stage promotes dense and uniform PbI_2 nuclei to ensure full-coverage crystal growth. The subsequent slow crystallization rate guarantees a crystallinity that will passivate inner defects.

4. Conclusion

The effects of relative humidity and airflow assisting on the PbI_2 solution deposition process, perovskite film crystalline structure and PSC performance were investigated. This work demonstrates that for vapor-assisted, two-step deposition processing of PSC, the quality of the perovskite film and the performance of the PSC device are critically determined by the precursor PbI_2 film. Spin coating PbI_2 at low RH benefits toward generating smooth and dense PbI_2 films with uniform porous holes to facilitate the growth of the perovskite crystals. The PSC device based on 16% RH-deposited PbI_2 film leads to a PCE of 8.6%. Airflow assistance during the PbI_2 deposition process can further improve surface morphology and crystallinity of CVD-grown perovskite films. Airflow-assisted spinning and drying steps improve solvent evaporation to get high supersaturation concentration, forming dense and uniform PbI_2 nuclei during the nucleation stage. The airflow-assisted thermal annealing step can retard the heating effect on PbI_2 films, slowing down the crystallization rate and passivating the inner defects. The PSC based on airflow-assisted PbI_2 films achieves a PCE of 12.4%, when fabricated with a low RH of 16%. These insights into the nucleation and crystallization processes of PbI_2 films may aid in further understanding PSC devices and in designing enhanced PSC devices.

Acknowledgments

This work was partially supported by the China Scholarship Council. The fabrication and characterization work were carried out in the Minnesota Nano Center and Characterization Facility, University of Minnesota.

ORCID iDs

Chongqiu Yang https://orcid.org/0000-0002-7042-6811
Tianhong Cui https://orcid.org/0000-0002-7427-2274

References

[1] Yang W S *et al* 2017 Iodide management in formamidinium-lead-halide–based perovskite layers for efficient solar cells *Science* **356** 1376–9
[2] Zhao Y and Zhu K 2016 Organic-inorganic hybrid lead halide perovskites for optoelectronic and electronic applications *Chem. Soc. Rev.* **45** 655–89
[3] Chiang C-H, Lin C-W and Wu C-G 2016 One-step fabrication of mixed-halide perovskite film for high-efficiency inverted solar cell and module *J. Mater. Chem.* A **4** 13525–33
[4] Jeon N J, Noh J H, Kim Y C, Yang W S, Ryu S and Seok S I 2014 Solvent engineering for high-performance inorganic-organic hybrid perovskite solar cells *Nat. Mater.* **13** 897–903
[5] Zhang X, Ye J, Zhu L, Zheng H, Liu G, Liu X, Duan B, Pan X and Dai S 2017 High-efficiency perovskite solar cells prepared by using a sandwich structure MAI-PbI_2-MAI precursor film *Nanoscale* **9** 4691–9
[6] Wu Y, Islam A, Yang X, Qin C, Liu J, Zhang K, Peng W and Han L 2014 Retarding the crystallization of PbI_2 for highly reproducible planar-structured perovskite solar cells via sequential deposition *Energy Environ. Sci.* **7** 2934–8
[7] Yin J, Qu H, Cao J, Tai H, Li J and Zheng N 2016 Vapor-assisted crystallization control toward high performance perovskite photovoltaics with over 18% efficiency in the ambient atmosphere *J. Mater. Chem.* A **4** 13203–10
[8] Guo Q, Li C, Qiao W, Ma S, Wang F, Zhang B, Hu L, Dai S and Tan Z A 2016 The growth of $CH_3NH_3PbI_3$ thin film by simplified close space sublimation for efficient and large dimensional perovskite solar cells *Energy Environ. Sci.* **9** 1486–94
[9] Peng Y, Jing G and Cui T 2015 A hybrid physical–chemical deposition process at ultra-low temperatures for high-performance perovskite solar cells *J. Mater. Chem.* A **3** 12436–42
[10] Zhu X, Yang D, Yang R, Yang B, Yang Z, Ren X, Zhang J, Niu J, Feng J and Liu S 2017 Superior stability for perovskite solar cells with 20% efficiency using vacuum co-evaporation *Nanoscale* **9** 12316–23
[11] Hsiao S-Y, Lin H-L, Lee W-H, Tsai W-L, Chiang K-M, Liao W-Y, Ren-Wu C-Z, Chen C-Y and Lin H-W 2016 Efficient all-vacuum deposited perovskite solar cells by controlling reagent partial pressure in high vacuum *Adv. Mater.* **28** 7013–9
[12] Hu H, Wang D, Zhou Y, Zhang J, Lv S, Pang S, Chen X, Liu Z, Padture N P and Cui G 2014 Vapour-based processing of hole-conductor-free $CH_3NH_3PbI_3$ perovskite/C_{60} fullerene planar solar cells *RSC Adv.* **4** 28964–7
[13] Liu M, Johnston M B and Snaith H J 2013 Efficient planar heterojunction perovskite solar cells by vapour deposition *Nature* **501** 395–8
[14] Yang D, Zhou X, Yang R, Yang Z, Yu W, Wang X, Li C, Liu S and Chang R P H 2016 Surface optimization to eliminate hysteresis for record efficiency planar perovskite solar cells *Energy Environ. Sci.* **9** 3071–8
[15] Chen Q, Zhou H, Hong Z, Luo S, Duan H-S, Wang H-H, Liu Y, Li G and Yang Y 2013 Planar heterojunction perovskite solar cells via vapor-assisted solution process *J. Am. Chem. Soc.* **136** 622–5
[16] Chen Q, Zhou H, Song T-B, Luo S, Hong Z, Duan H-S, Dou L, Liu Y and Yang Y 2014 Controllable self-induced passivation of hybrid lead iodide perovskites toward high performance solar cells *Nano Lett.* **14** 4158–63
[17] Cao X, Zhi L, Li Y, Fang F, Cui X, Yao Y, Ci L, Ding K and Wei J 2017 Control of the morphology of PbI_2 films for efficient perovskite solar cells by strong Lewis base additives *J. Mater. Chem.* C **5** 7458–64
[18] Yang C, Simon T and Cui T 2017 Numerical simulation and analysis of hybrid physical-chemical vapor deposition to grow uniform perovskite $MAPbI_3$ *J. Appl. Phys.* **121** 144903
[19] Cao X, Li Y, Fang F, Cui X, Yao Y and Wei J 2016 High quality perovskite films fabricated from Lewis acid-base adduct through molecular exchange *RSC Adv.* **6** 70925–31
[20] Wu C-G, Chiang C-H, Tseng Z-L, Nazeeruddin M K, Hagfeldt A and Gratzel M 2015 High efficiency stable inverted perovskite solar cells without current hysteresis *Energy Environ. Sci.* **8** 2725–33
[21] Liu T *et al* 2016 Mesoporous PbI_2 scaffold for high-performance planar heterojunction perovskite solar cells *Adv. Energy Mater.* **6** 1501890
[22] Hwang K, Jung Y S, Heo Y J, Scholes F H, Watkins S E, Subbiah J, Jones D J, Kim D Y and Vak D 2015 Toward large scale roll-to-roll production of fully printed perovskite solar cells *Adv. Mater.* **27** 1241–7
[23] Berhe T A, Su W-N, Chen C-H, Pan C-J, Cheng J-H, Chen H-M, Tsai M-C, Chen L-Y, Dubale A A and Hwang B-J 2016 Organometal halide perovskite solar cells: degradation and stability *Energy Environ. Sci.* **9** 323–56
[24] Gao H, Bao C, Li F, Yu T, Yang J, Zhu W, Zhou X, Fu G and Zou Z 2015 Nucleation and crystal growth of organic–inorganic lead halide perovskites under different relative humidity *ACS Appl. Mater. Inter.* **7** 9110–7
[25] Wozny S, Yang M, Nardes A M, Mercado C C, Ferrere S, Reese M O, Zhou W and Zhu K 2015 Controlled humidity study on the formation of higher efficiency formamidinium lead triiodide-based solar cells *Chem. Mater.* **27** 4814–20
[26] Gao L-L, Li C-X, Li C-J and Yang G-J 2017 Large-area high-efficiency perovskite solar cells based on perovskite films dried by the multi-flow air knife method in air *J. Mater. Chem.* A **5** 1548–57
[27] Huang F, Dkhissi Y, Huang W, Xiao M, Benesperi I, Rubanov S, Zhu Y, Lin X, Jiang L and Zhou Y 2014 Gas-assisted preparation of lead iodide perovskite films consisting of a monolayer of single crystalline grains for high efficiency planar solar cells *Nano Energy* **10** 10–8
[28] Dkhissi Y, Huang F, Rubanov S, Xiao M, Bach U, Spiccia L, Caruso R A and Cheng Y-B 2015 Low temperature processing of flexible planar perovskite solar cells with efficiency over 10% *J. Power Sources* **278** 325–31
[29] Mukhopadhyay M and Dalvi S V 2005 Analysis of supersaturation and nucleation in a moving solution droplet with flowing supercritical carbon dioxide *J. Chem. Technol. Biotechnol.* **80** 445–54

[30] Cronin H M, Jayawardena K I, Stoeva Z, Shkunov M and Silva S R P 2017 Effects of ambient humidity on the optimum annealing time of mixed-halide Perovskite solar cells *Nanotechnology* **28** 114004
[31] Gangishetty M K, Scott R W and Kelly T L 2016 Effect of relative humidity on crystal growth, device performance and hysteresis in planar heterojunction perovskite solar cells *Nanoscale* **8** 6300–7
[32] Cao X B, Li C L, Zhi L L, Li Y H, Cui X, Yao Y W, Ci L J and Wei J Q 2017 Fabrication of high quality perovskite films by modulating the Pb-O bonds in Lewis acid-base adducts *J. Mater. Chem.* A **5** 8416–22
[33] Li C, Tscheuschner S, Paulus F, Hopkinson P E, Kießling J, Köhler A, Vaynzof Y and Huettner S 2016 Iodine migration and its effect on hysteresis in perovskite solar cells *Adv. Mater.* **28** 2446–54
[34] Chen B, Yang M, Priya S and Zhu K 2016 Origin of J–V hysteresis in perovskite solar cells *J. Phys. Chem. Lett.* **7** 905–17
[35] Snaith H J, Abate A, Ball J M, Eperon G E, Leijtens T, Noel N K, Stranks S D, Wang J T-W, Wojciechowski K and Zhang W 2014 Anomalous hysteresis in perovskite solar cells *The Journal of Physical Chemistry Letters* **5** 1511–5
[36] Chiang C-H and Wu C-G 2016 Bulk heterojunction perovskite–PCBM solar cells with high fill factor *Nat. Photon.* **10** 196–200
[37] Xu J, Buin A, Ip A H, Li W, Voznyy O, Comin R, Yuan M, Jeon S, Ning Z and McDowell J J 2015 Perovskite-fullerene hybrid materials suppress hysteresis in planar diodes *Nat. Commun.* **6** 7081
[38] Meloni S *et al* 2016 Ionic polarization-induced current-voltage hysteresis in $CH_3NH_3PbX_3$ perovskite solar cells *Nat. Commun.* **7** 10334
[39] Chen S, Wen X, Sheng R, Huang S, Deng X, Green M A and Ho-Baillie A 2016 Mobile ion induced slow carrier dynamics in organic–inorganic perovskite $CH_3NH_3PbBr_3$ *ACS Appl. Mater. Inter.* **8** 5351–7
[40] Venables J A 2000 *Introduction to Surface and Thin Film Processes* (Cambridge, UK: Cambridge University Press)